
Proceedings Paper:
Sun, J. and Zhou, C. (2025) Advancing Robotic Jumping with CVT Enhanced SEA. In: Towards Autonomous Robotic Systems. 25th Annual Conference Towards Autonomous Robotic Systems (TAROS), 21-23 Aug 2024, London, UK. Lecture Notes in Computer Science (Part 1). Springer, Cham, Switzerland, pp. 73-84. ISBN: 978-3-031-72061-1. ISSN: 0302-9743. EISSN: 1611-3349.

https://doi.org/10.1007/978-3-031-72062-8_7

Advancing Robotic Jumping with CVT Enhanced SEA

Jingcheng Sun and Chengxu Zhou

***Abstract*—Series-elastic actuation (SEA) is widely employed on hopping robots due to its capability to diminish energy consumption and peak torque requirements. However, scant attention has been given in existing studies to the jump height achieved by robots utilizing SEA. To maximise jump height while retaining SEA's benefits, a solution to improve the actuator involves having a variable mechanical advantage (MA) gearbox between the elastic element and the end-effector. Continuously variable transmission (CVT) can produce such a precise MA profile with relatively straightforward structures. Although previous studies have incorporated CVT in robotics, with a predominant focus on wheeled robots, the potential advantages of using CVT on jumping robots have been overlooked. In this study, mathematical modelling is utilized to simulate and analyse the advantages of having a CVT-enhanced SEA (C-SEA) in terms of achieving higher jumps and protecting structural integrity for hopping robots. The results indicate that the C-SEA manages to reduce the peak ground reaction force by approximately 50% compared to the regular SEA. Moreover, C-SEA demonstrates superior performance in most cases with higher motor rotor mass and viscous damping coefficient when actuated by a motor with linear behaviour.**

***Index Terms*—Robotic jumping, Continuously variable transmission, Series-elastic actuators, Legged robots**

I. Introduction

Series-elastic actuation (SEA) is frequently used in robots designed for continuous hopping [1], [2] due to its ability to reduce energy consumption and peak torque requirements [3]. During continuous hopping, the elastic element can absorb and store the energy from the last jump as the robot lands and releases it into the next jump. However, previous studies on robots that use SEA often emphasize their agility rather than jump height. This preference stems from the common use of parallel-elastic actuators (PEA) to achieve high jumps for their ability to preload the spring during the flight phase [4]. Nonetheless, PEAs do not have the aforementioned benefits of energy conservation and torque reduction, making an SEA with enhanced jump capability the ideal actuator for hopping robots.

To optimise jump height while retaining the advantages of an SEA, the Salto robot provides a solution to improve the power modulation ratio (ratio between peak power output from a mechanism and that of its actuator) by having a linkage system with variable mechanical advantage (MA) as its leg mechanism [5]. However, the design process of a linkage system requires complex kinematic tuning to produce a desired MA profile. In contrast, a continuously variable transmission (CVT) can produce the same MA profile with much simpler structures. Furthermore, while the Salto robot does manage to improve the peak power output of the jumping mechanism, this enhancement does not directly contribute to the jump height, which is determined by the upward velocity of the robot body at the moment of leaving the ground. Therefore, the exact manner in how having varying MA increases the jump height of SEA-actuated hoppers needs to be further researched.

Previous studies have also incorporated CVT in robotics [6], [7], but they often focus on wheeled robots instead of legged ones. Some studies utilise CVTs with compliance as the method of changing MA [8], [9] but hardly any combine them with a SEA. One study investigates a CVT-SEA combination [10], mainly focusing on the control strategy for such actuators instead of specific scenarios for jumping application. Hence, the concept of CVT-enhanced SEA is novel for robotic jumping and necessitates mathematical modeling and simulation to evaluate its performance. The primary contributions of this paper are:

1) A theoretical continuously variable transmission gearbox that can be incorporated into series-elastic actuators for robotic jumping.
2) Mathematical models for the hopping robot powertrain, including the CVT gearbox and a simplified model for an electric motor powered prismatic actuator suitable for iterative simulation.
3) Comparative simulation studies to examine the performances of both the C-SEA and regular SEA in various scenarios. The advantages and limitations of the mechanism are analysed.

The structure of the paper is as follows. In Section. II, how to approach the analysis of a CVT-enhanced SEA is discussed; the structure of the hopping robot's powertrain is defined and the design criteria are specified. Section III introduces the mathematical models of the powertrain, the CVT gearbox, and the electric motor powered prismatic actuator; the constants that are later used in the simulation are also calculated from the design criteria. In Section. IV, two simulations are done: simulation 1 examines the general behaviours of the mechanisms when being powered by an ideal actuator; simulation 2 uses the full motor model to evaluate the effects on the height performance by specific variables. Section. V concludes the paper, and the planned future work is illustrated in this section.

Authors are with the School of Mechanical Engineering, University of Leeds, UK. c.x.zhou@leeds.ac.uk

This work was supported by the Royal Society [grant number RG\R2\232409].

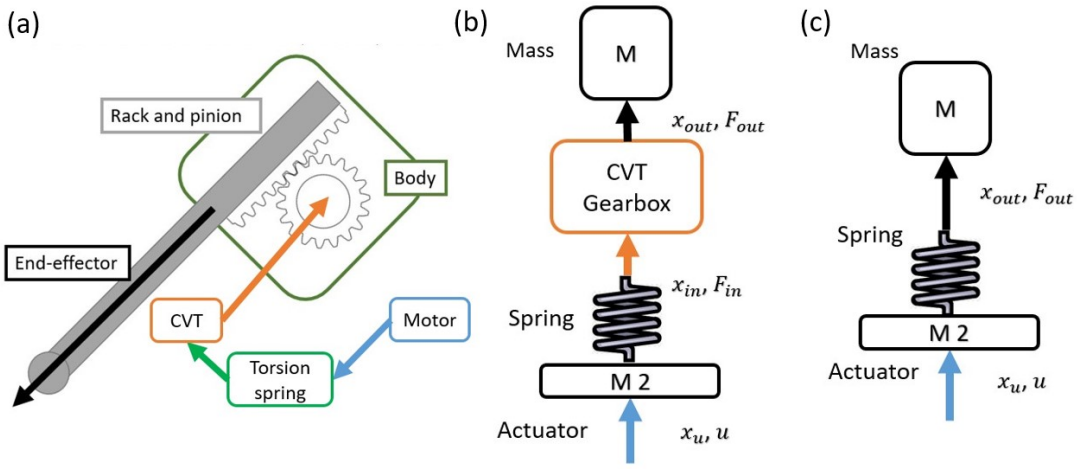

Fig. 1. A simplified structure of a hopping robot with C-SEA (a) and the isolated powertrains. Scenario (b) is the powertrain with a CVT and (c) is for a conventional SEA.

II. Methodology

To simulate a CVT-enhanced SEA robotic jumping, the advantages of having a mechanism between the elastic element and the end-effector with variable MA need to be analysed and understood. First of all, by aligning the MA profile and the spring's linear behaviour, the end-effector can produce almost constant force output, which reduces the peak ground reaction force. At the same time, having a high MA at the beginning of a stroke allows the spring to be fully compressed, thus it stores maximum energy to be released during the remainder of the stroke [5]. The first advantage improves structural integrity and reduces the material requirements for the leg mechanism, and the second one enables the robot to achieve higher jumps. This varying MA "gearbox" can be in the form of a CVT gearbox that can produce a precise MA profile that exactly matches the behaviour of the spring.

Generally in simulation, the structure of the device needs to be simplified enough so it can be mathematically defined. As shown in Fig. 1 (a), the hopper consists of a body and a leg mechanism for locomotion, with the powertrain contained inside the body. In a realistic scenario, the powertrain only provides angular motion; then, it is converted into linear motion by a rack-and-pinion mechanism. However, to avoid any complex dynamic model, the powertrain of the jumper is isolated and linearised. In Fig. 1 (b) and (c), the mass M represents the robot body and m_2 is the mass of moving components in a motor; the corresponding behaviours of each section of the powertrain are denoted by the letters on the side. In the linearised model, the motion of the robot body relative to the ground is simply represented by that of the mass M with respect to the surroundings. Since the primary objective of utilising the C-SEA is to maximise jump height, there should be a target height for the robot to reach, a fixed body mass and a maximum stroke length for the end-effector. In this case, the design criteria for the robot with a body mass of 100 g is to jump to 1 m with a stroke length (x_{max}) of 0.2 m. The parameters are averages from past light-weight jumping robots like Salto [5], EPFL jumper [11] and MSU jumper [12]; the numbers are adjusted to be mathematically convenient. The variable v_{max} is defined as the velocity of the robot body at the lift-off (the end of a stroke where the end-effector is no longer touching the ground) which directly determines the height the jump can reach. In this model, only the one dimensional vertical motion of the robot is concerned. However, balancing mechanisms such as AeroTail [13] can be easily added to allow locomotion due to its structural simplicity.

III. Mathematical Modelling

Following the assumptions made in Section.II, mathematical models for the powertrain and the CVT gearbox can be derived. Some initial conditions that will be useful in the simulation are also provided by the models. Additionally, a model for a realistic electric motor is provided in this section.

A. Powertrain and CVT models

The characteristics of CVTs compared to regular gearboxes with variable gear ratios is that a CVT can adjust gear ratio in a smooth range instead of fixed steps. Therefore, how the gear ratio changes is very flexible and open to imagination. For the simplicity of modelling, the CVT gearbox has linear inputs and outputs in the forms of displacement and force instead of angles and torques. Still using the powertrain structure in Fig.1 (b) and assuming the spring used has perfectly linear behaviour, the input force (F_{in}) can be calculated using:

$$F_{in} = k(x_u - x_{in}) \tag{1}$$

where k is the spring constant, x_u is the displacement of the actuator and x_{in} is the input displacement into the gearbox. The gear ratio ($Gr(x_{in})$) of the CVT is set to be a linear function of the input displacement:

$$Gr(x_{in}) = G_0 - R \cdot x_{in} \tag{2}$$

where G_0 and R are constants according to the properties of the CVT gearbox. In this case, the mechanical advantage (M_A) of the gearbox is simply the inverse of the gear ratio:

$$M_A = \frac{1}{Gr(x_{in})} = \frac{1}{G_0 - R \cdot x_{in}}. \tag{3}$$

Therefore, the output displacement (x_{out}) and the output force (F_{out}) from the gearbox can also be calculated:

$$\begin{aligned} x_{out} =& \int Gr(x_{in})\, dx_{in} = G_0 x_{in} - \frac{1}{2} R x_{in}^2 \\ F_{out} =& F_{in} \cdot M_A = \frac{k(x_u - x_{in})}{G_0 - R \cdot x_{in}} \end{aligned} \tag{4}$$

and the dynamic behaviour of the powertrain can be simulated using Euler method in later sections.

B. Constants calculation

Using the design criteria and assumptions made in Section.II, constants from equations (1) to (4) can be calculated and used as known values later on in the simulations. Given the stroke length x_{max}, target height and mass of the robot body, the ideal spring constant k, and target v_{max} can be calculated using the conservation of mechanical energy:

$$\begin{aligned} U_1 =& U_2 = U_3 \\ mgh =& \frac{1}{2} k (x_{max})^2 = \frac{1}{2} m (v_{max})^2 \end{aligned} \tag{5}$$

where U_1 is the potential energy from height, U_2 is that from the compressed spring and U_3 is the kinetic energy of the mass at the end of the stroke. In this model, drag and damping are assumed to be negligible. Thus, the ideal spring constant can be calculated as 49.05 N/m; the target v_{max} is 4.43 m/s; and the fully compressed spring produces a force of 9.81 N (denoted by F_0). To generate a constant output force, this condition has to be true:

$$\frac{dF_{out}}{dx_{in}} = 0, \tag{6}$$

and thus we get relations:

$$\frac{F_0}{G_0} = \frac{k}{R} \tag{7}$$

where F_0 and k are known. If we assume the total output stroke length is the same as the input one, the remaining two constants can be calculated: $G_0 = 2$ and $R = 10$. When the CVT consists of conical rollers, R directly reflects the slope of the cones; when it does allow the gearbox to have a mechanical advantage profile that produces constant output force, it is named the "critical gear ratio constant". For clarity and realism, the R used in the simulation is 9.9, slightly smaller than the critical gear ratio constant.

C. Motor model

Various previous works have used a standard model for electric motors [3], [14]. The linearised version of the equations is illustrated below:

$$\begin{aligned} V =& L\frac{dI}{dt} + RI + kv \\ I =& \frac{F + k_m v}{k} \end{aligned} \tag{8}$$

where L is the terminal inductance, R is the winding resistance and k is the motor's back EMF constant with a unit of $N \cdot A^{-1}$ (newton over ampere); V, I, F are the voltage input, current and the motor force output respectively. Compared to their original counterpart, several modifications have been made. Motor constant k no longer has a unit of Nm/A since it is linearised and describes the relation between the input voltage and the v (unit m/s) instead of the angular velocity ω (unit s^{-1}). At the same time, the motor torque output T_m is changed to simply force F. From (8), the expression of the motor's force output as a function of its velocity can be derived:

$$F = (\frac{k_m}{k})V - k_m v \tag{9}$$

where v is the motor velocity and k_m is a constant known as the viscous damping coefficient. It can be calculated using:

$$k_m = \frac{kI_0}{v_0} \tag{10}$$

where v_0 and I_0 are the no load velocity and current. Since the input voltage is assumed to be constant, (9) can be further simplified to:

$$F = F_0 - k_m v \tag{11}$$

where F_0 is the "stall force" of the motor (same as the maximum spring force).

IV. Simulation

Two simulation studies are done in this section. Simulation 1 is to showcase the general behaviour of the C-SEA with a single end-effector stroke intending to propel the robot body to the target height. The output accelerations and velocities are compared with their SEA counterparts in specific scenarios. Simulation 2 studies the factors that can affect the v_{max} achieved by the actuators in question and the results from various input combinations are compared and analysed. The simulations in this study are exclusively done in MATLAB using the Euler method with a time step of 0.1 millisecond.

A. Simulation 1

An important characteristic of the C-SEA is producing reduced and almost constant output force, and this is enabled by the gear ratio being a linear function of the input displacement. To showcase this feature, a kinematic simulation of the CVT gearbox is done. The governing equation of the behaviour is based on (4) with some modifications. We assume the system is not actuated but simply powered by a compressed spring and only the analytic outputs of the gearbox are being examined (masses are ignored); thus in this case, x_u is a fixed value

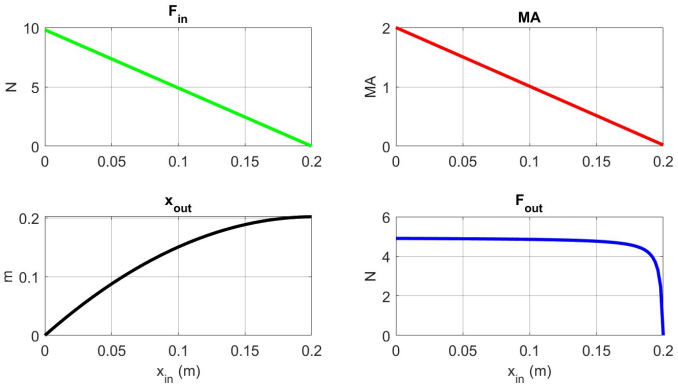

Fig. 2. The results from the kinematic simulation. The input force (F_{in}), mechanical advantage (MA), end-effector position (x_{out}) and output force (F_{out}) are plotted against the input displacement (x_{in}).

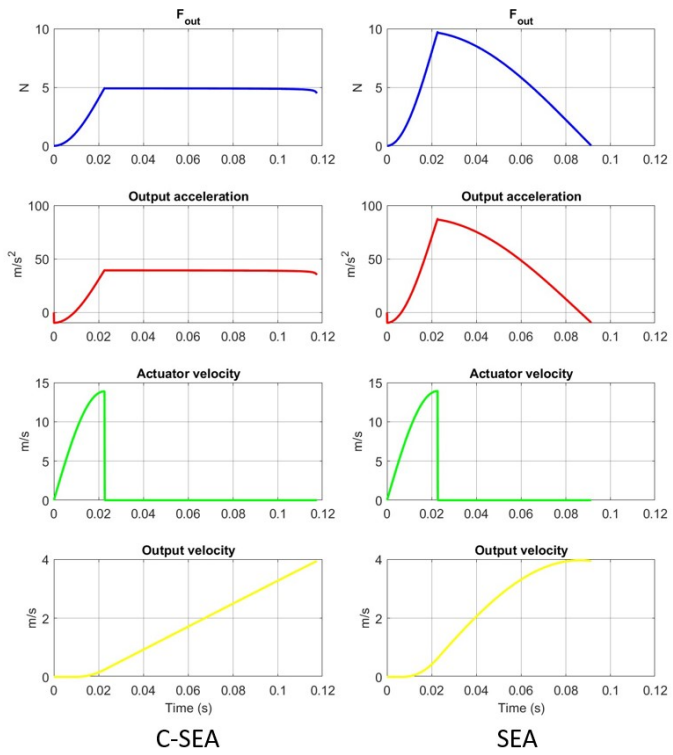

Fig. 3. The results from the dynamic simulation. The output force (F_{out}), acceleration and velocity along with the actuator velocity are plotted against time. Since the mass remains unchanged, F_{out} and the acceleration have the same shape.

of x_{max}. If we plug in the constants from Section. III-B, the behaviour of the system in a single stroke is plotted with respect to input displacement x_{in} in Fig. 2. The output force is kept nearly constant and only drops at the end of the stroke with a peak value of 4.91N, half of the peak input force of 9.81N.

The next step is to simulate the full dynamic behaviour of both the C-SEA and the regular SEA according to the powertrain structure in Fig 1 and the mathematical model in Section III. The powertrain is placed along the vertical

TABLE I
SUMMARY OF SIMULATION 1 RESULTS

Scenarios	v_{max}(m/s)	Time(s)	Height(m)	Peak force(N)
Ideal scenario	4.43	–	1.000	9.81
C-SEA actuated	3.93	0.117	0.787	4.91
SEA actuated	3.97	0.091	0.803	9.81

direction with the full effect of gravity. m_2 is set to be 10g and the actuator is assumed to generate constant force with no limit on velocity. The maximum extent of x_u is constrained to x_{max} and the lift-off happens when the output displacement reaches x_{max}. The results are demonstrated in Fig. 3 where the x-axis is now time. The C-SEA experiences almost constant output acceleration thus linear velocity and ground reaction force throughout the stroke with a peak value around half of its SEA counterpart. The results also show that the stroke have two stages, the charging and the releasing, in a continuous manner which sees end-effector starting to displace as the spring is being compressed.

The summarised results can be found in Table I. The system with C-SEA takes 0.117 s to reach a velocity of 3.93 m/s while the one without CVT takes 0.091 s to achieve a velocity of 3.97 m/s. C-SEA takes longer to reach the end velocity but v_{max} and thus jump height is only slightly affected (0.787 m for C-SEA and 0.803 m for SEA). Therefore, without the CVT, a regular SEA would have produced 99.8% more peak ground reaction force while reducing the time duration by 22.1%. However, this simulation result still cannot reflect a realistic scenario since the actuator, if being powered by an electric motor, simply cannot generate perfectly constant force output while having no velocity limitation. The maximum velocity reached by the actuator, as shown in Fig. 3, is a whopping 13.87 m/s which is an unrealistically big number. To make the simulation more realistic, the mathematical model for the electric motor introduced in Section. III-C should be included in the overall model.

B. Simulation 2

As discussed in Section. II, the second advantage arises from the initial high MA at the beginning of the stroke and a lower MA at the end, which allows for more thorough compression of the spring, thereby storing greater energy for achieving higher jumps. The rationale behind it is that prolonged charging stages can lead to premature expansion of the spring, resulting in incomplete compression when energy is released. However, the results from Section. IV-A show that the conventional SEA still outperforms in terms of jump height. This largely attributes to the assumption that the ideal actuator produces constant force with unlimited velocity, which is unrealistic and causes the charging stage to be shorter than if an electric motor is powering the actuator.

When considering an actuator powered by a linear electric motor, the time required to compress the spring is influenced by two factors: m_2 and k_m. The first factor is self-explanatory, as larger masses are harder to accelerate according to Newton's

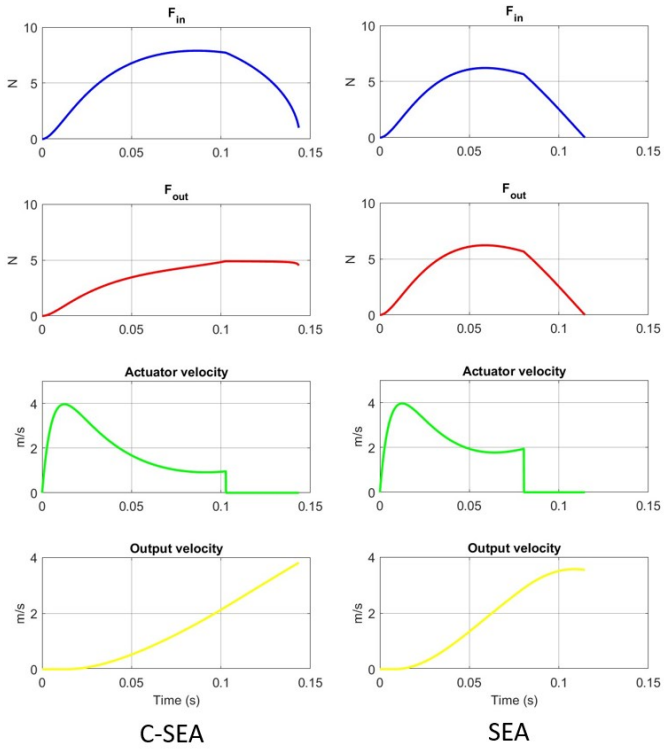

Fig. 4. The results of simulation 2. The input force from spring (F_{in}), output force (F_{out}), actuator velocity and the end-effector velocity are plotted against time. Since there is no gearbox in SEA, its (F_{in}) and (F_{out}) are identical here.

second law. The second factor determines how much the force output from the motor decreases as it speeds up. If the actuator has a linear behaviour, the charging will take longer; this consequently causes the spring to prematurely expand. When using the C-SEA, this premature expansion would be mitigated by the high MA at the beginning of the stroke, thus allowing the robot to reach a better height.

To prove the addition of the motor model in Section. III-C does affect the performance in the manner described above, the general behaviour of the system with the new model is simulated. The k_m is set to be 2 so that when the stall force is F_0, the no-load velocity of the actuator is 4.9 m/s slightly larger than the required v_{max}; everything else remains unchanged from the setup of the dynamic Simulation 1. The results can be found in Fig. 4. As expected, the peak force output from C-SEA is still way less than the input even though the constant section is shorter compared to Simulation 1; SEA still takes less overall time to complete the stroke. A major difference from the previous simulation is that the peak force output now is only slightly higher than its C-SEA counterpart which is precisely caused by the spring in SEA not being fully compressed during the charging stage. Consequently, the v_{max} achieved by C-SEA this time is 3.81 m/s, exceeding the 3.57 m/s of the SEA. This proves the notion mentioned previously: when using a realistically modelled actuator with linear behaviour, the C-SEA still manages to compress the spring fairly well during the charging stage which is now longer, while the conventional performs poorly.

To further study the effects of m_2 and k_m on v_{max} for both C-SEA and SEA, combinations of the variables from wide ranges are used to produce a 3D plot of the results (in Fig. 5). m_2 has a range from 1 g to 100 g; the lower bound is a number small enough to represent the lowest possible value for the mass of the moving component in the actuator but still easy enough to simulate, while the upper bound is the mass of the robot body which is impossible to exceed. At the same time, k_m ranges from 0 to 5. When $k_m = 0$, $F = F_0$; this represents the scenario in simulation 1 where the actuator produces constant force. Lastly, the end-effector fails to complete a full stroke when k_m exceeds 5, thus the upper bound. The values for the variables are distributed in an exponential manner throughout the ranges, and the results are plotted in 3D. Two best-fit surfaces are generated for both the C-SEA and the SEA using the "polyfit23" function. The contours of the surfaces are also shown in Fig. 5. The red dotted line divides the contours in two regions, most m_2 and k_m combinations to the top-right of the red line, see higher v_{max} for C-SEA. This indicates that for motors with both larger m_2 and k_m, the C-SEA usually have a clear advantage over the regular SEA.

V. Conclusion and Future Works

In conclusion, the C-SEA manages to generate nearly constant and lower ground reaction force than the regular SEA sacrificing the time taken to accelerate with minimal loss on jump height. The reduced ground force is beneficial to the structural integrity and means less material requirements for the end-effector. At the same time, when actuated by a realistic motor, C-SEA has a clear advantage in most cases with higher m_2 and k_m outperforming the SEA in terms of achieving high jumps because of the C-SEA's ability to compress the spring more thoroughly even when the charging stage is extended.

For future work, the findings in the paper will facilitate the development of a physical CVT gearbox that can be integrated with an SEA for robotic jumping and a prototype of such C-SEA enabled hopping robot will be constructed. Next steps for this research include: choosing a CVT type, parameter optimization for the CVT, designing and fabricating the hopping robot as a testing platform, developing a control strategy for such a robot and finally conducting comparative experiments. Promising CVT options include Evan's variable speed counter-shaft and the ratcheting CVT; the former boasts a simple and reliable structure, while the latter excels in transmitting impressive torque with minimal loss [15]. Furthermore, a monopedal hopping robot inevitably needs flight-phase balance control when the leg mechanism has only one degree of freedom. Ultimately, combining hopping with other locomotion methods such as gliding [16] could yield a versatile robot suitable for inspecting extreme environments inaccessible to humans.

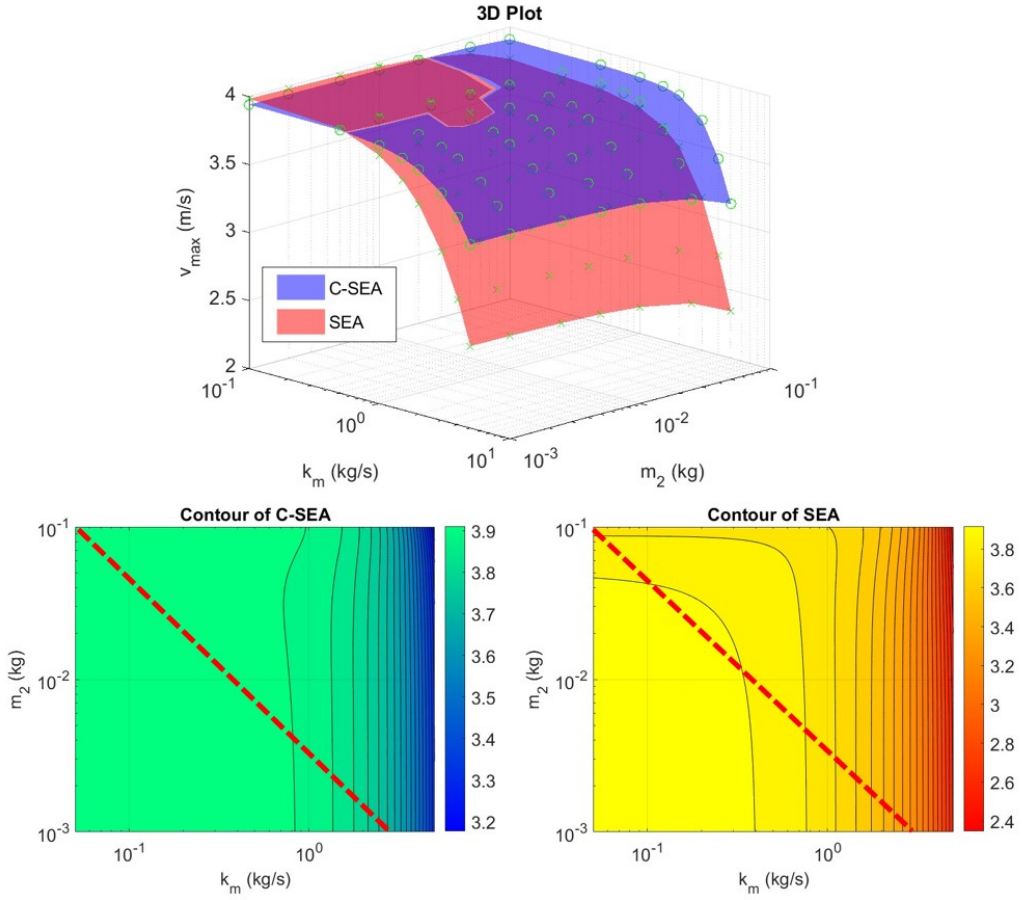

Fig. 5. The 3D plots for the results from simulation 2 are on the top and their corresponding contours are also shown on the bottom. The endpoints of the red dotted line have Cartesian coordinates $[0, 0.1]$ and $[3, 0.001]$ in the contour plots. The dotted line divides the regions according to whether C-SEA or SEA has the better performance.

REFERENCES

[1] N. Csomay-Shanklin, V. D. Dorobantu, and A. D. Ames, "Nonlinear model predictive control of a 3D hopping robot: Leveraging lie group integrators for dynamically stable behaviors," in *IEEE International Conference on Robotics and Automation*, pp. 12106–12112, 2023.

[2] W. D. Shin, W. Stewart, M. A. Estrada, A. J. Ijspeert, and D. Floreano, "Elastic-actuation mechanism for repetitive hopping based on power modulation and cyclic trajectory generation," *IEEE Transactions on Robotics*, vol. 39, no. 1, pp. 558–571, 2022.

[3] P. Beckerle, T. Verstraten, G. Mathijssen, R. Furnémont, B. Vanderborght, and D. Lefeber, "Series and parallel elastic actuation: Influence of operating positions on design and control," *IEEE/ASME Transactions on Mechatronics*, vol. 22, no. 1, pp. 521–529, 2016.

[4] M. Grimmer, M. Eslamy, S. Gliech, and A. Seyfarth, "A comparison of parallel-and series elastic elements in an actuator for mimicking human ankle joint in walking and running," in *IEEE International Conference on Robotics and Automation*, pp. 2463–2470, 2012.

[5] M. M. Plecnik, D. W. Haldane, J. K. Yim, and R. S. Fearing, "Design exploration and kinematic tuning of a power modulating jumping monopod," *Journal of Mechanisms and Robotics*, vol. 9, no. 1, p. 011009, 2017.

[6] J. Kim, F. C. Park, and Y. Park, "Design, analysis and control of a wheeled mobile robot with a nonholonomic spherical CVT," *The International Journal of Robotics Research*, vol. 21, no. 5-6, pp. 409–426, 2002.

[7] A. S. Kernbaum, M. Kitchell, and M. Crittenden, "An ultra-compact infinitely variable transmission for robotics," in *IEEE International Conference on Robotics and Automation*, pp. 1800–1807, 2017.

[8] K. Matsushita, S. Shikanai, and H. Yokoi, "Development of Drum CVT for a wire-driven robot hand," in *IEEE/RSJ International Conference on Intelligent Robots and Systems*, pp. 2251–2256, 2009.

[9] A. A. Nobaveh, J. L. Herder, and G. Radaelli, "A compliant continuously variable transmission (cvt)," *Mechanism and Machine Theory*, vol. 184, p. 105281, 2023.

[10] L. Mooney and H. Herr, "Continuously-variable series-elastic actuator," in *IEEE International Conference on Rehabilitation Robotics*, pp. 1–6, 2013.

[11] M. Kovač, O. Fauria, J.-C. Zufferey, D. Floreano, *et al.*, "The epfl jumpglider: A hybrid jumping and gliding robot with rigid or folding wings," in *2011 IEEE International Conference on Robotics and Biomimetics*, pp. 1503–1508, IEEE, 2011.

[12] J. Zhao, J. Xu, B. Gao, N. Xi, F. J. Cintron, M. W. Mutka, and L. Xiao, "Msu jumper: A single-motor-actuated miniature steerable jumping robot," *IEEE Transactions on Robotics*, vol. 29, no. 3, pp. 602–614, 2013.

[13] J. Sun and C. Zhou, "AeroTail: A bio-inspired aerodynamic tail mechanism for robotic balancing," in *The 28th International Conference on Automation and Computing*, pp. 436–441, 2023.

[14] J. Pentzer and S. Brennan, "Investigation of the effect of continuously variable transmissions on ground robot powertrain efficiency," in *American Control Conference*, pp. 4245–4250, 2012.

[15] F. Benitez, J. Madrigal, and J. Del Castillo, "Infinitely variable transmission of racheting drive type based on one-way clutches," *Journal of Mechanical Design*, vol. 126, no. 4, pp. 673–682, 2004.

[16] J. Sun, J. Yang, R. Richardson, and C. Zhou, "Gliding mechanism with hinged aeroelastic wings," in *The 5th UK-RAS Conference*, pp. 80–81, 2022.